

## Properties of hydrogen induced voids in silicon

This article has been downloaded from IOPscience. Please scroll down to see the full text article.

2005 J. Phys.: Condens. Matter 17 S2303

(<http://iopscience.iop.org/0953-8984/17/22/019>)

View [the table of contents for this issue](#), or go to the [journal homepage](#) for more

Download details:

IP Address: 129.252.86.83

The article was downloaded on 28/05/2010 at 04:55

Please note that [terms and conditions apply](#).

# Properties of hydrogen induced voids in silicon

J Weber, T Fischer, E Hieckmann, M Hiller and E V Lavrov

Institute for Applied Physics/Semiconductor Physics, TU Dresden, 01062 Dresden, Germany

Received 6 October 2004

Published 20 May 2005

Online at [stacks.iop.org/JPhysCM/17/S2303](http://stacks.iop.org/JPhysCM/17/S2303)

## Abstract

After heat treatment, silicon samples implanted with high doses of hydrogen exhibit blistering and defoliation of thin silicon layers. The process is used commercially in the fabrication of thin silicon-on-insulator layers (Smart Cut<sup>®</sup>). In the present study we investigate the behaviour of hydrogen after different processing steps, which lead to thin Si layers bonded to glass substrates. A set of hydrogen implanted samples is studied by means of low temperature photoluminescence, Raman spectroscopy, x-ray diffraction and optical microscopy (visible and infrared). The formation of Si–H bonds is detected after implantation together with a build-up of internal strain. After annealing, the relaxation of the implanted layers is found to be connected with the formation of hydrogen saturated vacancies and the formation of H<sub>2</sub> molecules filling up larger voids. A comparison is made with hydrogen plasma treated samples, where well defined platelets on {111} planes are found to trap hydrogen molecules. No direct evidence of the role of {111} and {100} platelets in the blistering process is found in the implanted layers from our study. We determine considerable compressive stresses in the bonded Si layers on glass substrates. The photoluminescence is strongly enhanced in these bonded layers but red-shifted due to a strain reduced band gap.

(Some figures in this article are in colour only in the electronic version)

## 1. Introduction

Ion implantation of high hydrogen doses into silicon crystals leads to blistering. Under certain conditions a thin Si film is separated from the surface. In 1995 this phenomenon was first suggested for the formation of thin crystalline films on insulators (silicon-on-insulator, SOI) [1]. The so-called Smart-Cut<sup>®</sup> technique involves bonding of the implanted donor wafer surface onto an oxidized Si wafer or other substrates [2]. A thermal treatment leads to the cracking of the donor wafer at the implantation depth of the ions and to the SOI structure on top of the substrate. The implantation parameters are crucial for the success of the technique. The kinetic energy determines the average penetration depth  $R_p$  in Si. For proton implantation into Si approximately 8 nm keV<sup>-1</sup> were reported [3]. For implantation doses of protons above

$D_{\text{H}}^+ > 2 \times 10^{17} \text{ cm}^{-2}$  blisters are directly generated at the surface of crystalline silicon. An increasing dose generates flakes of crystalline Si from the surface. For implantation doses in the range  $D_{\text{H}}^+ = 1 \times 10^{16} - 2 \times 10^{17} \text{ cm}^{-2}$  blistering occurs only after heat treatment of the implanted sample. Below this dose a blistering was never detected even after more elaborate heating cycles [4]. Systematic studies on the formation kinetics of the blisters revealed the formation time dependence on dose, annealing temperature, silicon surface orientation and doping concentration [2, 5–7]. The formation of the blisters sets in abruptly. At the so-called onset time the blisters pop up and are visible at the surface [8].

Implantation of ions into Si creates extended lattice defects, with the highest concentration in the range of the average penetration depth  $R_p$ . The implanted hydrogen is mostly bound in these defect structures, leading to different Si–H or Si–H<sub>2</sub> vibrational modes [3, 4, 9, 10].

In several transmission electron microscopy (TEM) studies extended defects (voids) were found within the penetration depth of the hydrogen. For a (100) implanted surface these extended defects are preferentially oriented along the (100) plane (some also along {111} planes). They exhibit an extension of a few 10 nm and a thickness of a few atomic layers [2, 10, 11]. These defect structures, which are also generated during hydrogen plasma treatments, are called platelets. Annealing leads to an increase of the platelet structures by Ostwald ripening and the final formation of the blisters. It is assumed that the hydrogen in the platelets forms H<sub>2</sub> molecules. Estimates for a blister with a diameter of 2  $\mu\text{m}$  and a height of 10 nm give an internal pressure of  $p_{\text{H}_2} \approx 1 \text{ GPa}$  which leads to the deformation of the crystal surface [10].

For bonding of the implanted wafer to a substrate, flat surfaces are required. Therefore blister formation directly during implantation has to be avoided by low doses of hydrogen. After bonding, a heat treatment leads to the splitting of the wafer pair [9]. Depending on the implantation dose the splitting occurs at  $R_p$  or at the depth of highest defect concentration [12]. The generation of microcracks and their kinetics are closely related to the development of the hydrogen induced defect structure. The present understanding of this process uses a critical diameter of the microcracks above which the propagation of the crack is driven by the high pressure of the hydrogen in the structure [13, 14]. The microscopic origin of the initial crack formation is not known. In particular, the involvement of hydrogen in the early stages of blistering is based on many speculations. However, the filling of larger cavities with molecular hydrogen during annealing is assumed in all models of the blistering process.

Hydrogen plasma treatment of silicon samples at room temperature leads to the formation of well defined platelets on {111} lattice planes. The platelets are stabilized by atomic hydrogen and a characteristic Si–H Raman line at  $2100 \text{ cm}^{-1}$  is associated with the hydrogen bonded to the Si internal surface atoms [15]. A successive filling of the platelets with H<sub>2</sub> molecules was detected at increasing annealing temperatures [16]. Blister formation was reported for sample temperatures of 400 °C or higher during plasma treatment [17].

A systematic study of hydrogen implanted Si(100) wafers will be presented. Several different optical methods were applied and in addition for internal strain determination x-ray diffraction was used.

## 2. Experimental details

The silicon samples used in this study were prepared from a p-type, boron doped, CZ(100) wafer with the resistivity of 2  $\Omega \text{ cm}$ . The wafer was covered with SiO<sub>2</sub> (150 nm). The sample series A were implanted with 129 keV H<sub>2</sub><sup>+</sup> at room temperature with a dose of  $2.5 \times 10^{16} \text{ cm}^{-2}$  (sample A1). Afterwards a sample of kind A1 was annealed for 10 h at 400 °C and additionally for 1 h at 500 °C in air (sample A2).

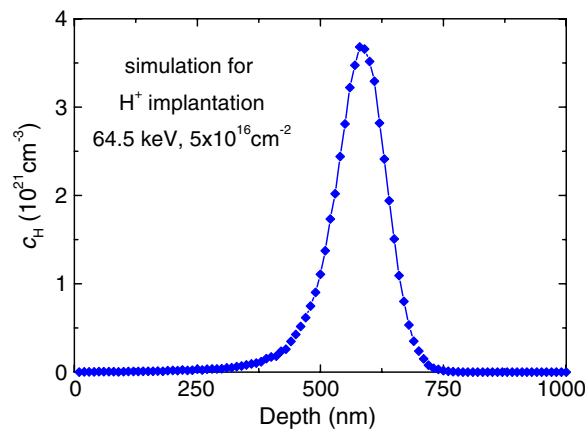


**Figure 1.** Calculated depth profile for  $H_2^+$  implantation, using the SRIM software.

**Table 1.** Sample parameters.

Series A	Si(001) single crystal p-type, boron doped, $2 \Omega \text{ cm}$
A1	Implantation with $H_2^+$ at room temperature $129 \text{ keV}/2.5 \times 10^{16} \text{ cm}^{-2}$
A2	After annealing (blistering) $400^\circ \text{C}$ (10 h) + $500^\circ \text{C}$ (1 h) in air
A3	Substrate after defoliation
A3top	Surface layer bonded to glass substrate

Another sample was bonded after implantation to a glass substrate. An annealing identical to that for A2 leads to the defoliation of the thin Si layer bonded to the glass substrate. A3 is the remaining wafer and A3top is the thin layer bonded to the glass substrate. Table 1 gives a list of the sample parameters.

We have performed SRIM calculations to determine the depth distribution of the H atoms after implantation [18]. It is believed that the  $H_2^+$  ion splits upon impact with the wafer surface, coming to rest as a hydrogen atom. The implantation of  $H_2^+$  is therefore equivalent to the implantation of  $H^+$  with half the energy 64.5 keV and twice the dose  $5 \times 10^{16} \text{ cm}^{-2}$  [5, 19]. Figure 1 gives the calculated profile for the implantation energy of 129 keV ( $H_2^+$ ).

Atomic force microscopy (AFM) was performed to determine the surface roughness and the size of the blisters. We used an Autoprobe M5 from ThermoMicroscopes in the non-contact mode. It was possible to determine the layer thickness of the thin bonded layers, although the accuracy of these measurements was not too good due to the lack of proper calibration of the depth scale.

The x-ray diffraction experiments were carried out at room temperature with  $\text{Cu K}\alpha_1$  radiation by a high resolution double-crystal diffractometer, equipped with a flat (111) Si monochromator. The diffracted intensity was measured with a position sensitive detector (for more details see [20]). The instrumental profile broadening is assumed to be negligible due to the applied focusing principle which was introduced by Guinier [21] and Wilkens [22]. For all the Si samples, Bragg diffraction profiles  $I(\theta)$  of 004 reflection type were measured within a Bragg angle interval of  $1.3^\circ$  with a step size  $\Delta\theta = 0.0004^\circ$ . While recording, the samples were moved across the full rocking curve interval. The profile tails were measured down to  $10^{-5}$  of the maximum intensity at most.

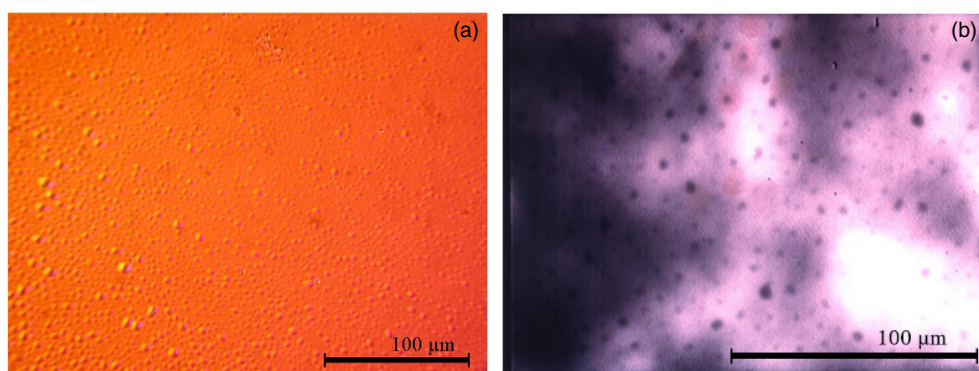


**Figure 2.** (a) Photograph of the surface of sample A2 under polarized visible light; (b) IR transmission—the unpolished back surface leads to a strong variation in the contrast. The sample areas are not the same in the two images.

Raman measurements were performed with the 488 nm line of an Ar<sup>+</sup>-ion laser for excitation. The focused incident laser beam made an angle of 50° with the sample surface. The laser was focused to a spot size of 50 μm onto the sample surface. The total laser power was 200 mW. The backscattered light was dispersed using a 0.3 m single-grating spectrometer and for detection a cooled silicon CCD detector array was used. The sensitivity of the set-up over the whole spectral region of interest remained constant within 5%. The position of the lines in the Raman spectra was calibrated using the Raman lines of atmospheric N<sub>2</sub> and O<sub>2</sub>. The spectral resolution was 7 cm<sup>-1</sup>. An appropriate holographic notch filter was used to reduce the scattered laser light. Polarized Raman spectra were collected in pseudo-backscattering geometry.

Photoluminescence (PL) was excited by the different lines of an Ar<sup>+</sup>-ion laser. All samples were mounted in a He bath cryostat at 4.2 K. The PL signals were analysed with a grating monochromator ( $f = 0.75$  m) and detected with a liquid nitrogen cooled Ge detector. The standard lock-in technique was used for signal processing.

### 3. Experimental results

#### 3.1. Microscopy

All samples were studied by optical microscopy in the visible and IR range (2 μm). The as-implanted samples show no surface structure and there is no contrast in the IR transmission of these samples. Figure 2 gives the photographs of sample A2 which was annealed after implantation. Blisters are visible in (a) with varying sizes; the average diameter was determined to be 4 μm, but the largest of the blisters reach up to 10 μm.

The small black dots in the IR transmission photograph, figure 2(b), are due to scattered light from the blisters. All dark spots are found to be at the same focus length of the microscope, indicating a very similar depth distribution.

The samples after the bonding process show large parts of thin surface regions which were not transferred to the glass substrate (figures 3 and 4). This is certainly due to the imperfect bonding procedure used for our samples. Figure 3 shows the substrate material with areas which were not transferred. Clearly in the non-transferred areas blisters are still visible.

The height distribution of the blisters was determined by standard scanning atomic force microscopy in non-contact mode. Figure 5 gives the results for sample A2. The maximum

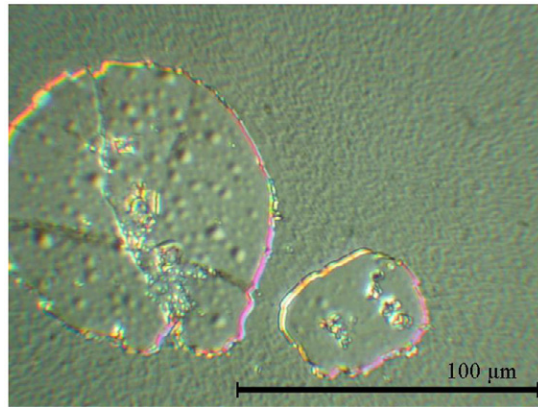


**Figure 3.** A3 remaining layer on top of the Si substrate after the ion cut.

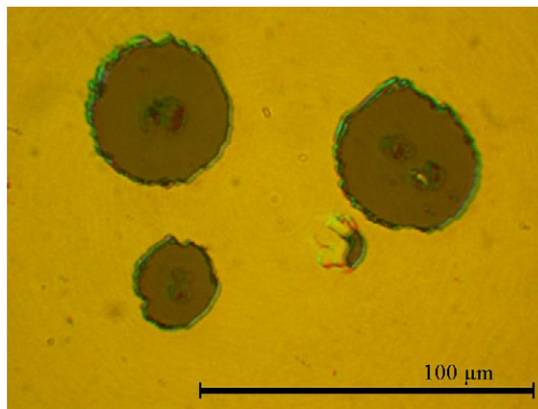


**Figure 4.** A3top layer on the glass substrate. The dark areas are holes in the transferred film.

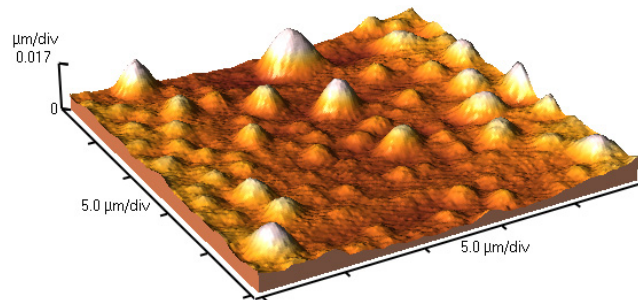


**Figure 5.** 3D projection of the AFM results for sample A2.

height detected for this sample was 50 nm. We determined the height of the remaining film (A3sp) on top of substrate A3 and compared this thickness with the thin film on the glass substrates (A3top).

In table 2 we summarize the results. The two values for the layer thickness seem to agree within the variations along the layer and indicate a splitting just above the implanted layer, where most of the implantation damage was created [9].

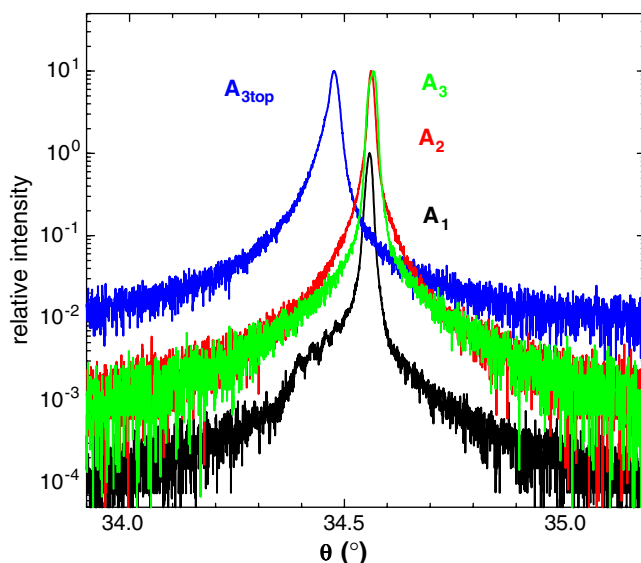


**Figure 6.** Diffraction profiles for sample series A. For sample A1 the relative intensity was multiplied by  $10^{-1}$ .

**Table 2.** Layer thickness determined by AFM, averaged over several measurements. Estimated error:  $\pm 20$  nm.

Spacing between	Thickness, $d$ (nm)
A3top and glass	450
A3sp and A3	430

### 3.2. X-ray diffraction

Typical Bragg diffraction profiles, measured in the vicinity of the 004 reflection, are shown in figure 6. In all samples the spots studied are crystalline. The integral breadth  $\beta(\theta)$  of the profile can be used as a rough estimate of the root mean square strain in the layers  $\langle \varepsilon_{\perp}^2 \rangle^{1/2}$  perpendicular to the sample surface. By applying the Stokes–Wilson relation [23] for profile shapes between Gaussian-like and Cauchy-like functions we can find

$$\beta(\theta) \approx \alpha \langle \varepsilon_{\perp}^2 \rangle^{1/2} \tan \theta_0$$

where  $\theta_0$  is the Bragg angle for the ideal crystal and  $\alpha$  is a factor, determined by the profile shape. For a pure Gaussian function  $\alpha = (2\pi)^{1/2}$  and for a Cauchy function  $\alpha \approx 0$ . Table 3 lists the results for all the samples. The thin top layer bonded to the glass substrate exhibits a pronounced increase of the rms strains, as can be directly seen from the strongly broadened Bragg reflex shown in figure 6. Taking into account the x-ray penetration depth of some micrometres in Si this behaviour of the profile is explainable because sample A3top is fully damaged whereas in the other samples the less damaged substrate reduces the profile broadening. As expected, the annealed substrate A3 after defoliation of the top layer shows the lowest, but noticeable, rms strains.

The shift ( $\theta_p - \theta_0$ ) of the Bragg peak indicates long range strain fields in the irradiated volume. Only for the sample A3top is a pronounced shift detected; all other samples show

**Table 3.** rms strains and macroscopic compressive residual stresses in the samples.

X-ray results	A1	A2	A3	A3top
$\alpha$	1.45	0.92	2.25	0.21
$\langle \varepsilon_{\perp}^2 \rangle^{1/2}$ ( $10^{-4}$ )	3.3	5.3	2.6	41.7
$\sigma$ (MPa)	-60	-10	0	-580

only smaller shifts—not resolvable within the scale of figure 6. We calculate from the peak shift the two-dimensional stress  $\sigma$  in the layers using

$$\bar{\varepsilon}_{\perp} = -(\theta_p - \theta_0) \cot \theta_0 \quad \text{and} \quad \sigma = \sigma_{11} = \sigma_{22} = \left[ -\frac{C_{11}^2}{2C_{12}} - \frac{C_{11}}{2} + C_{12} \right] \bar{\varepsilon}_{\perp}$$

where the  $C_{ij}$  are the elastic moduli [24]. As expected, due to the implantation of H into the Si lattice the layer is compressed. The stress is relaxed after annealing and after lift-off. Our data support the general view that hydrogen implantation into Si results in the formation of an in-plane compressive stress. This in-plane compressive stress is accompanied by an out-of-plane tensile strain distribution [9, 25].

Evidently, in the bonded layer a high compressive stress is found. The bonding of the layers is performed at 500 °C, and during cooling down to room temperature the different thermal expansion coefficients of glass and Si lead to the highly compressive stress in the Si layer.

For sample A1 a pronounced shoulder as well as some oscillations on the lower side of the Bragg peak diffraction angle occur. Similar oscillations were found after H<sup>+</sup> implantation in boron doped [001] Si wafers [26]. The oscillations can be interpreted as thickness fringes caused by the damaged layer due to implantation. The number of thickness fringes is a demonstration of the lateral homogeneity of the layer thickness. The width and the oscillation period  $\delta\theta$  of the fringes are related to the inverse of the layer thickness  $L$ , and in a rough kinematic approximation  $L$  can be estimated using the following equation [27]:

$$L \approx \lambda / 2\delta\theta \cos \theta_0,$$

with  $\lambda$  the x-ray wavelength ( $\lambda = 0.1541$  nm). According to our data we derive an average thickness of  $L = 190$  nm for sample A1, which is in good agreement with the calculated hydrogen depth profile shown in figure 1.

### 3.3. Raman studies

Typical room temperature Raman spectra of samples A1 and A2 are presented in figure 7. Only the spectral range of the Si–H stretch local vibrational modes (LVM) is shown. Very pronounced sharp lines are seen for both samples; they are superposed for sample A1 on a broad band centred at  $\sim 2000$  cm<sup>-1</sup>. A detailed Raman analysis was performed on similar samples and was published in [28]. In particular, the polarized Raman spectra allowed a correlation of LVMs with the infrared absorption and EPR studies of [29–31]. Most of the defects responsible for the lines in figure 8 are vacancy–hydrogen complexes; the labels in figure 7 indicate the nature of the underlying defect. During implantation, vacancies are created which can bind the implanted hydrogen. Annealing of the samples after implantation leads to the disappearance of the broad band and a shift in intensity of the different complexes. In sample A2, complexes which include more hydrogen or more vacancies are preferentially formed.

Two lines in the spectra are labelled Si–H, according to the similarities to IR lines reported in [10, 32]. The LVM at 1957 cm<sup>-1</sup> was identified in [33] as a complex involving a Si interstitial



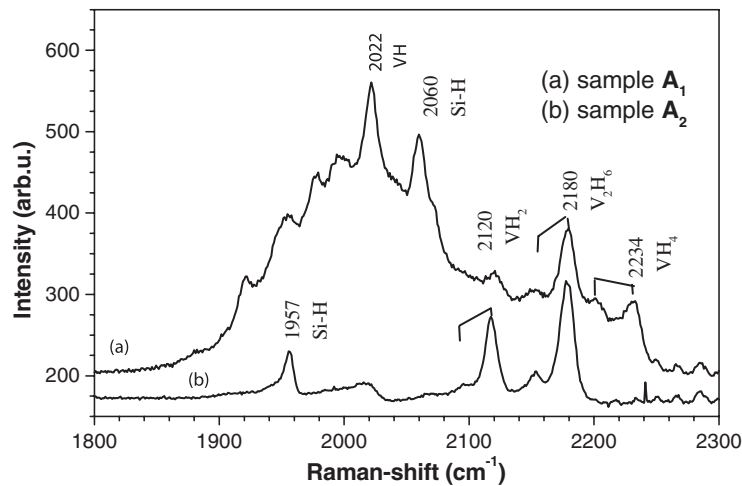


**Figure 7.** Raman spectra measured at room temperature. (a) As-implanted sample A1, (b) annealed and blistered sample A2.

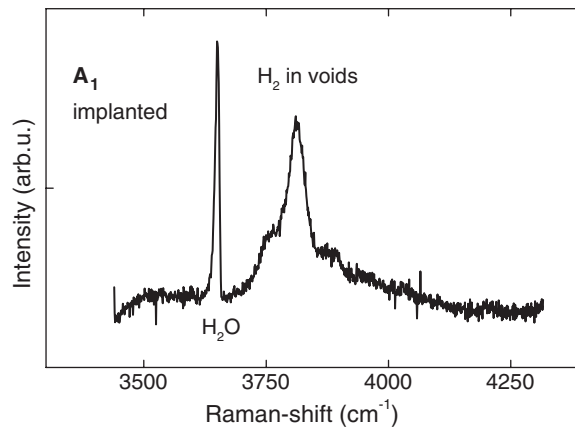


**Figure 8.** Raman spectra of sample A1. The line at  $3650\text{ cm}^{-1}$  is due to a LVM of atmospheric water vapour.

and two hydrogen atoms (I-H<sub>2</sub>). This defect seems to be stable against annealing at  $500\text{ }^{\circ}\text{C}$ . The LVM at  $2060\text{ cm}^{-1}$  is one of the dominant lines in the as-implanted samples. A clear relation with data from the literature is not possible. Tentatively, we give the interpretation of [10] where a connection is made to Si-H vibrations at internal surfaces.

Samples A3 (substrate) and the top layer on glass (A3top) give identical Raman spectra to sample A2. In these samples the broad band is missing and only the sharp lines of sample A2 are detectable with very similar relative intensities. This behaviour indicates that part of the implantation damage is created much deeper and lower than the projected range in accordance with the x-ray diffraction results. The lines in the substrate and the bonded layer are therefore not directly related to the mechanism of the blistering. However, the comparison of the spectra with that of A1 clearly shows the development of larger and more hydrogen filled defects (VH<sub>4</sub> in A2 instead of VH in A1).

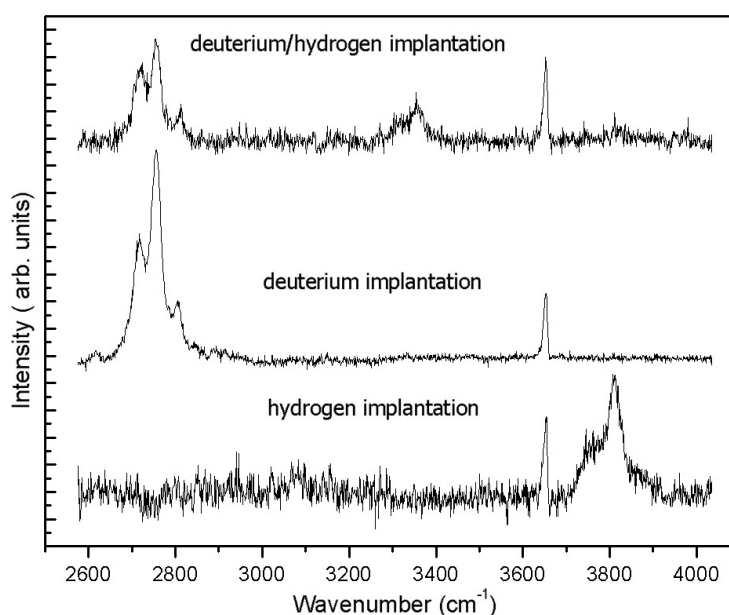


**Figure 9.** LVM from samples implanted with hydrogen, deuterium and a deuterium/hydrogen mixture.

The broad Raman band at  $2000\text{ cm}^{-1}$  seems to correlate with H trapped in a highly defective Si region and could therefore give a solution to the blistering mechanism. As was pointed out by Weldon and co-workers [10] this broad band is very reminiscent of that observed for hydrogenated amorphous silicon (a:Si-H), which was attributed to an inhomogeneous distribution of monohydride-terminated, multivacancy defects of the form  $V_xH_y$  with  $x = 3$  or 4 and  $y = 1$  [34]. The polarized Raman studies clearly point to a trigonal symmetry of the defect centres responsible for the broad band.

The band at  $2100\text{ cm}^{-1}$ , which is reminiscent of  $\{111\}$  platelets created by plasma treatment, is not detected for the hydrogen implanted samples. The  $H_2$  signal at  $4150\text{ cm}^{-1}$  characteristic for the  $\{111\}$  platelets filled with  $H_2$  is also missing for our samples. However, for sample A1 a new broad signal is found at  $3810\text{ cm}^{-1}$ . Figure 8 shows the band, which exhibits a clear structure with shoulders. The additional sharp line in the spectrum of figure 8 is due to water vapour close to the surface of the sample.

In figure 9 the spectrum of this broad band is given for a sample which was implanted with hydrogen, deuterium or both species at the same time. The implantation conditions were similar to those for sample A1. A clear shift of the line at  $3810\text{ cm}^{-1}$  is seen for deuterium implantation whereas the mixed implantation creates a band at  $3350\text{ cm}^{-1}$ . This behaviour is typical for hydrogen molecules and indeed the broad band has been assigned recently to hydrogen molecules in voids [35, 36]. The polarization of the  $H_2$  band with respect to the crystallographic orientation and the incoming laser beam indicates a freely rotating  $H_2$  molecule in larger voids. On the basis of the present measurements we cannot rule out the possibility that the voids are related to the (100) platelets. Further studies are needed to unravel the nature of the  $3810\text{ cm}^{-1}$  band.

The  $H_2$  signal supports the general view of the generation of blisters. The high pressure exerted by hydrogen in the microvoids leads at high enough temperatures to the surface blistering.

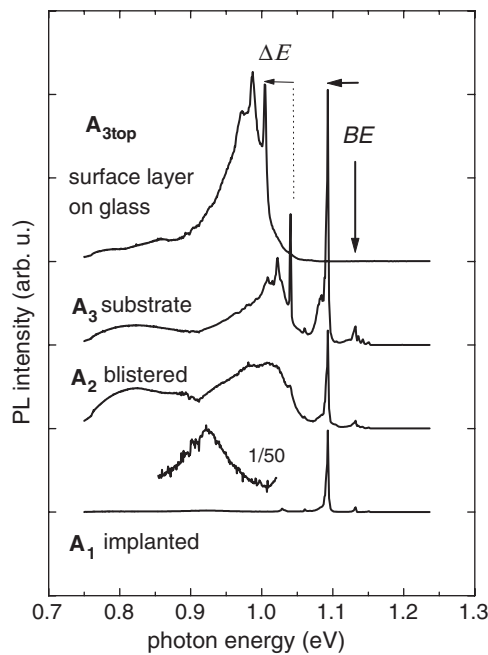


**Figure 10.** Low temperature PL spectra ( $T = 4.2$  K).

#### 4. Photoluminescence results

The low temperature PL spectra of the samples are given in figure 10. Sample A1 exhibits the bound exciton (BE) recombination typical for a boron doped sample. A weak, broad band at 921 meV is the only indication of the implantation process. This band was attributed recently to a radiative recombination at  $\{311\}$  defects [37]. The PL intensity of the BE increases with the penetration depth of the laser (from  $\lambda_{\text{exc}} = 457.9\text{--}647.1$  nm by a factor of 3) indicating that the damaged surface layer is smaller than the penetration depth of the red laser line.

Sample A2 shows a significantly different PL spectrum. A broad PL band dominates the spectrum. On the high energy site of the band a sharp, weak PL line appears at 1039 meV. This line is seen in more clarity for sample A3. The associated phonon structure and the energy position identify this line as the  $I_3$  or X centre [38, 39]. The broadband PL is reduced in this sample. The linewidths of the  $I_3$  line are very similar for the two samples, supporting the results of the x-ray measurements: a very similar random strain distributions in these samples.

In the layer bonded to the glass substrate A3top we detect no BE luminescence from the band edge region, e.g. the boron BE. However, the remaining PL intensity is clearly increased compared to those for samples A1 and A2. This is a typical behaviour of thin luminescent layers, where the exciton concentration is increased due to the increased exciton localization. For sample A3top the  $I_3$  spectrum is shifted towards smaller energies by  $\Delta E = 36$  meV. No variations in the spectral position of  $I_3$  with the excitation spot are detected. The linewidth is increased compared to that for sample A3 only by a factor 2.

We interpret the large shift of  $I_3$  for sample A3top in terms of a large in-plane compressive stress. The splitting of the  $I_3$  line under uniaxial stress was determined in [40]. If we use the measured stress splitting we find a compressive stress in the layer of 1.09 GPa. This internal stress in the layer has to be compared to the value determined from the x-ray diffraction

which is roughly half the size (0.56 GPa). Although the two stresses were determined by different methods (x-ray and photoluminescence) a much better agreement as regards the value is expected. However, there is a major difference in the stress values determined. The x-ray measurements were performed at room temperature whereas the PL measurements had to be performed at 4.2 K. This large temperature dependence of the stress field in the layer hints at the origin of the internal stress field. The layer was bonded to the glass substrate at 400 °C; at that temperature the interface was stress free. Due to the different thermal expansion coefficients of glass and Si a high internal compressive strain field is generated during cooling down of the bonded layer on glass. The glass substrate is much thicker than the Si layer, which leads to a highly strained Si layer, with the strain field parallel to the interface. Under the assumption of linear thermal expansion coefficients we derive from the room temperature x-ray data a low temperature value of the internal stress of 1.16 GPa, close to the value determined from the stress splitting of the  $I_3$  line.

## 5. Summary

Room temperature implantation of hydrogen at doses below  $5 \times 10^{16} \text{ cm}^{-2}$  leads to a highly compressed layer perpendicular to the implantation direction. The damaged region leads to a broad Raman signal at  $2000 \text{ cm}^{-1}$  and a PL band at 921 meV. Several sharp lines in the Raman and PL spectra originate from areas above and below the damaged region. The Raman lines can be associated with well known vacancy or interstitial–hydrogen complexes. A Raman band at  $3810 \text{ cm}^{-1}$  is attributed to  $\text{H}_2$  in larger voids. However, the nature of these voids is not known. The broad features in the Raman measurements at  $2000$  and  $3810 \text{ cm}^{-1}$  as well as the 921 meV band in PL disappear after annealing the samples at 400 °C. The remaining sharp Raman lines belong to larger vacancy or interstitial clusters containing several hydrogen atoms. The dominant PL line  $I_3$  for these samples was recently attributed to a small interstitial cluster.

The Raman and PL measurements are in agreement with the general belief that the blistering is associated with the formation and filling of voids with  $\text{H}_2$ . The voids in the implanted samples are clearly different from the  $\{111\}$  platelets detected in plasma treated samples. At present we cannot exclude or support the idea that the blisters are connected to  $\{100\}$  platelets.

In Si layers bonded to glass a high compressive stress is generated due to the different thermal expansion coefficients.

In conclusion, the hydrogen implantation leads to a broad Raman line at  $2000 \text{ cm}^{-1}$  which is spatially located in the highly damaged region. This line was correlated with vibrational modes of hydrogen in vacancy clusters in a-Si. TEM investigations verify the amorphous layer structure of  $\{100\}$  platelets. The  $\text{H}_2$  signal was found for the implanted samples at  $3810 \text{ cm}^{-1}$ . Unfortunately the polarization dependence of this signal gives no clear information on the symmetry of the void. Blistering leads to the disappearance of the broad signal at  $2000 \text{ cm}^{-1}$  and also of the  $\text{H}_2$  signal, indicating a process where the hydrogen pressure leads to an increase in size of the voids and a final blistering. Further measurements are needed to unravel the nature of the voids.

## Acknowledgments

L-J Huang carefully prepared most of the samples used in this study at the Wafer Bonding Laboratory at Duke University, Durham (NC). B Bech Nielsen implanted deuterium in several

Si samples. Special thanks are due to U Gösele for stimulating discussions. We thank B Köhler for technical assistance during the experiments. This work was partially supported by the BMBF under contact 05KK10DA/2.

## References

- [1] Bruel M 1995 *Electron. Lett.* **31** 1201
- [2] Bruel M 1998 *MRS Bull.* **23** 35
- [3] Chu W K, Kastl R H, Lever R F, Mader S and Masters B J 1977 *Phys. Rev. B* **16** 3851
- [4] Maleville Chr, Aspar B, Poumeyrol T, Moriceau H, Bruel M, Auberton-Hervé A J and Barge T 1997 *Mater. Eng. B* **46** 14
- [5] Tong Q-Y, Gutjahr K, Hopfe S, Gösele U and Lee T-H 1997 *Appl. Phys. Lett.* **70** 1390
- [6] Zheng Y, Lau S S, Höchbauer T, Misra A, Verda R, He X-M, Nastasi M and Mayer J W 2001 *J. Appl. Phys.* **89** 2972
- [7] Aspar B, Moriceau H, Jalaguier E, Lagahe C, Soubrie A, Biasse B, Papon A M, Claverie A, Grisolia J, Benassayag G, Letertre F, Rayssac O, Barge T, Maleville C and Ghyselen B 2001 *J. Electron. Mater.* **30** 834
- [8] Huang L-J, Tong Q-T, Chao Y-L, Lee T-H, Martini T and Gösele U 1999 *Appl. Phys. Lett.* **74** 982
- [9] Höchbauer T, Misra A, Nastasi N and Mayer J W 2001 *J. Appl. Phys.* **89** 5980
- [10] Weldon M K, Marsico V E, Chabal Y J, Agarwal A, Eaglesham D J, Sapjeta J, Brown W L, Jacobson D C, Caudano Y, Christman S B and Chaban E E 1997 *J. Vac. Sci. Technol. B* **15** 1065
- [11] Grisolia J, Ben Assayag G, Claverie A, Aspar B, Lagahe C and Laanab L 2000 *Appl. Phys. Lett.* **76** 852
- [12] Höchbauer T, Misra A, Nastasi N and Mayer J W 2002 *J. Appl. Phys.* **92** 2335
- [13] Han W and Yu J 2001 *J. Appl. Phys.* **89** 6551
- [14] Yang F 2003 *J. Appl. Phys.* **94** 1454
- [15] Johnson N M, Ponce F A, Street R A and Nemanich R J 1987 *Phys. Rev. B* **35** 4166
- [16] Lavrov E V and Weber J 2001 *Phys. Rev. Lett.* **87** 185502
- [17] Wang L, Fu R K Y, Zeng X and Chu P K 2001 *J. Appl. Phys.* **90** 1735
- [18] Ziegler J F 2003 The stopping and range of ions in matter, Version SRIM-2003.10. URL <http://www.SRIM.org>
- [19] Cerofolini G F, Meda L, Volpones C, Ottaviani G, Defayette J, Dierckx R, Donelli D, Orlandini M, Anderle M, Canteri R, Claeys C and Vanhellemont J 1990 *Phys. Rev. B* **41** 12607
- [20] Hecker M, Thiele E and Holste C 1997 *Z. Metallk.* **88** 321
- [21] Guinier A and Sébilleau F 1952 *C. R. Acad. Sci.* **235** 888
- [22] Wilkens M and Eckert K 1964 *Z. Naturf. a* **19** 459
- [23] Stokes A R and Wilson A J C 1944 *Proc. R. Soc.* **56** 174
- [24] Noyan I C and Cohen J B 1987 *Residual Stress—Measurement by Diffraction and Interpretation* (New York: Springer)
- [25] Cerofolini G F, Meda L, Balboni R, Corni F, Frabboni S, Ottaviani G, Tonini R, Anderle M and Canteri R 1992 *Phys. Rev. B* **46** 2061
- [26] Miclaus C and Goorsky M S 2003 *J. Phys. D: Appl. Phys.* **36** A177
- [27] Bellet D and Dolino G 1997 X-ray diffraction studies of porous silicon *Structural and Optical Properties of Porous Silicon Nanostructures* ed G Amato, C Delerue and H-J von Bardeleben (Amsterdam: Gordon and Breach)
- [28] Lavrov E V, Weber J, Huang L and Bech Nielsen B 2001 *Phys. Rev. B* **64** 035204
- [29] Bech Nielsen B, Stallinga P, Bonde Nielsen K and Byberg J R 1997 *Phys. Rev. Lett.* **79** 1507
- [30] Bech Nielsen B, Hoffmann L and Budde M 1996 *Mater. Sci. Eng. B* **36** 259
- [31] Bech Nielsen B and Grimmeiss H G 1989 *Phys. Rev. B* **40** 12403
- [32] Weldon M K, Collot M, Chaball Y J, Venezia V C, Agarwal A, Haynes T E, Eaglesham D J, Christman S B and Chaban E E 1998 *Appl. Phys. Lett.* **73** 3721
- [33] Budde M, Bech Nielsen B, Leary P, Goss J, Jones R, Briddon P R, Öberg S and Breuer S J 1997 *Mater. Sci. Forum* **258–263** 35
- [34] Pearton S J, Corbett J W and Stavola M 1992 *Hydrogen in Crystalline Semiconductors* (Berlin: Springer)
- [35] Ishioka K, Kitajima M, Tataeishi S, Nakanoya N, Fukata N, Mori T, Murakami K and Hishita S 1999 *Phys. Rev. B* **60** 10852
- [36] Mori T, Otsuka K, Umehara N, Ishioka K, Kitajima M, Hishita S and Murakami K 2001 *Physica B* **302** 239
- [37] Coffa S, Libertino S and Spinella C 2000 *Appl. Phys. Lett.* **76** 321
- [38] Davies G, Lightowlers E C and Ciechanowska Z E 1987 *J. Phys. C: Solid State Phys.* **20** 191
- [39] Coomer B J, Goss J P, Jones R, Öberg S and Briddon P R 2001 *J. Phys.: Condens. Matter* **13** L1
- [40] Ciechanowska Z, Davies G and Lightowlers E C 1984 *Solid State Commun.* **49** 427